JOURNAL OF MATERIALS SCIENCE 17 (1982) 3549–3563

A compliant, high failure strain, fibre-reinforced glass-matrix composite

KARL M. PREWO
United Technologies Research Center, East Hartford, Connecticut 06108, USA

It is demonstrated that a unique form of composite material can be achieved by reinforcing glass matrices with discontinuous graphite fibres. The graphite fibres were utilized in the form of a paper, purchased in large sheets, and composites were formed by hot-pressing glass-powder-impregnated paper plys. The resultant composites exhibit high strength, high fracture toughness (compared to ceramics), low density and low thermal expansion coefficient. Of particular note is the unique tensile stress–strain curve achieved which exhibits both high strength and high failure strain. Its very non-linear shape differs markedly from that of either the unreinforced glass or a similarly reinforced epoxy-matrix composite. In addition, the elastic modulus of the resultant composite, despite being reinforced with a high stiffness fibre, is lower than that of the parent matrix resulting in an unusually compliant ceramic material.

1. Introduction

The continuing need for advanced materials in high-performance engineering systems has led scientists to the conclusion that crystalline ceramics and oxide glasses offer many advantages over metal alloys. For gas turbines and diesel engines, ceramics have been chosen because of their high-temperature strength, environmental stability and relative low density. In high-performance optical systems oxide glasses have been selected for use because of their exceptional dimensional stability. In both of these and other situations, however, the use of these materials is severely limited by their extreme sensitivity to flaws and generally brittle character. Recent efforts have attempted to overcome these limitations through the use of continuous fibre reinforcement. By using silicon carbide fibres to reinforce glasses [1, 2] and glass-ceramics [3] it has been possible to achieve materials whose strength, environmental stability and toughness show great potential for use in heat engines. Similarly, the use of continuous graphite fibres to reinforce glasses has succeeded in providing dimensionally stable materials with excellent strength, stiffness and toughness [4–8]. One attempt at using discontinuous graphite fibres as reinforcement demonstrated that a random array could indeed achieve toughening but not an increase in strength over the parent matrix [9]. It required the use of aligned discontinuous fibres to achieve both strengthening and toughening. While these successful continuous fibre-reinforced glass-matrix composites can be shown to be an outgrowth of high-performance fibre-reinforced resins technology, it will be shown in this paper that another very different approach can also be taken to achieve reliable ceramics and glasses.

The field of fibre-reinforced plasters, cements and concretes has, for many years, demonstrated that fibre-reinforcement can significantly alter the stress–strain behaviour of brittle materials. More recently there has been considerable activity in explaining how this use of even small percentages of all manner of fibres can transform a fragile, brittle material into one useful in general construction [10, 11]. Of particular significance is the ability to create high failure strain composites whose tensile stress–strain curves are highly non-linear despite the very limited strain capability of both matrix and fibre. Tensile stress–strain curves of the form shown in Fig. 1 have led to the ability of these construction materials to redistribute applied loads in a manner similar to metals and

0022–2461/82/123549–15$04.30/0

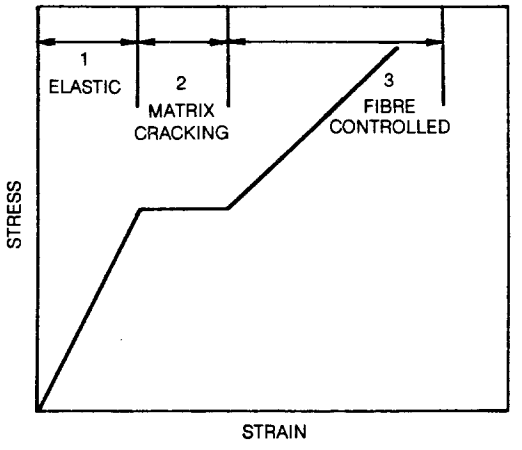

Figure 1 Idealized tensile stress–strain curve for a fibre-reinforced cement [10, 11].

hence achieve greater reliability. The three principal regions in this curve correspond to the following.

Region 1 – Both fibre and matrix deform elastically.

Region 2 – At some proportional limit stress, the matrix undergoes microcracking while the fibres bridge the cracks and take up the extra stress. Ideally the propagation of these microcracks throughout the specimen gauge length occurs at a level of constant applied stress until a critical crack spacing has been achieved.

Region 3 – Matrix cracking has stopped and additional strain is carried by the fibres to the point of final fibre, and hence composite, fracture.

It will be shown in this paper that a tensile stress–strain curve related to this form can be obtained for discontinuous graphite fibre-reinforced glass. Unlike the case of continuous fibre reinforcement, the discontinuous fibre-reinforced system exhibits an elastic modulus less than that of the starting matrix and a distinct proportional limit followed by additional stress increase prior to fracture. It is thus a demonstration of the ability to create a compliant, relatively high failure strain ceramic suitable for high-performance applications.

2. Experimental procedure

2.1. Composite fabrication

All composites were fabricated through the use of thin sheets of discontinuous graphite fibre paper. This apper consists of a two-dimensional array of in-plane randomly oriented fibres held together by approximately 5 to 10% by weight of organic binder (generally polyester). It was obtained in 91 cm wide continuous length rolls from the International Paper Company, Tuxedo Park, New York, USA, and in 25 cm square sheets from the C. H. Dexter Co of Windsor Locks, Connecticut, USA. The fibres in each type of paper were of constant length and individually separated so that the paper consisted of an array of fibres and not fibre bundles. Except where noted, all of the data presented in this study were obtained from glass-matrix composites reinforced with fibres that were 1.9 cm in length prior to composite densification. Measurement of fibre *in situ* length was not made to ascertain whether extensive fibre breakage had occurred during hot pressing.

Composite fabrication consisted of cutting individual plys of the desired shape out of the paper and touching each ply to a bunsen burner flame to remove the binder. The plys were then dipped into a slurry of glass powder suspended in propanol followed by drying and placement in a graphite die cavity for hot pressing. All plys were aligned during lay-up to keep their original orientation colinear with regard to the paper roll axis. Composite panels were fabricated in 7.5 cm × 7.5 cm and 10 cm × 10 cm sizes by hot-press densification of these fibre plus glass powder arrays using 6.9 MPa pressure at temperatures above 1200° C.

The glass matrices and graphite fibres used are listed in Table I along with their properties. The three glasses provide a wide range of high-temperature stability and thermal expansion characteristics

TABLE I Starting-material properties

	Density ($g\,cm^{-3}$)	Elastic modulus (GPa)	Tensile strength (MPa)	Annealing point (°C)	Coefficient of thermal expansion ($10^{-6}\,°C^{-1}$)
Borosilicate glass	2.23	63	–	560	3.25
Aluminosilicate glass	2.64	88	–	710	4.60
96% silica glass	2.18	67	–	910	0.8
PR-286 epoxy	1.27	4.1	–	–	66.0
Celion fibre	1.76	234	2760	–	–
Fortafil 5 fibre	1.77	350	2700	–	–

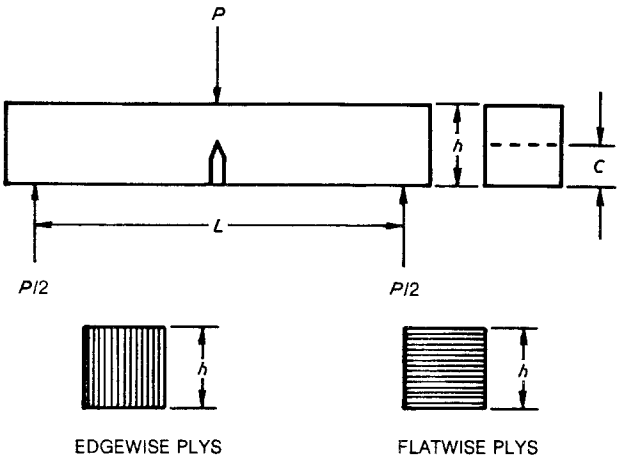

Figure 2 Notched and unnotched three-point bend specimens with two ply configurations.

while the two fibres differ primarily in elastic modulus. The epoxy properties are included for purposes of later discussion.

2.2. Test specimens

Test specimens were prepared from the panels by cutting and grinding with a diamond abrasive wheel. Three-point bend specimen configurations are shown in Fig. 2 where the notations for specimen test span (L), specimen depth (h), and in the case of notched specimens, notch depth (c) are indicated. The notch-tip radius was 125 μm. Also shown in the figure are two ply orientations tested, edgewise and flatwise. In the former case the original plys are located on edge with regard to the direction of applied load, while in the latter the load is applied normal to the ply plane. In the case of three-point bend testing the overall specimen dimensions were 7.5 cm x 0.5 cm x 0.2 cm for large span-to-depth ratios, 5.5 cm x 0.5 cm x 0.5 cm for small span-to-depth ratios, and 10 cm overall length, 0.5 cm wide, 0.2 cm thick, with a 2.5 cm gauge length for tensile testing.

Glass fibre-reinforced epoxy doublers were provided for tensile gripping. Except where noted, all specimens were presurface ground to remove excess surface glass that resulted from fabrication.

3. Experimental results for Celion graphite reinforced borosilicate glass

3.1. Composite microstructure

The resultant composite microstructure is shown in Fig. 3 where it can be seen that the fibres retained a two-dimensional distribution; no fibres are oriented normal to the original paper plys. Although some small fibre groupings are observable in the figure, it is also clear that the fibres are primarily individually distributed rather than in their original tows or bundles. The Celion graphite-reinforced borosilicate composites consisted of approximately 30 to 35% by volume of graphite fibres, 1 to 3% by volume porosity, and the

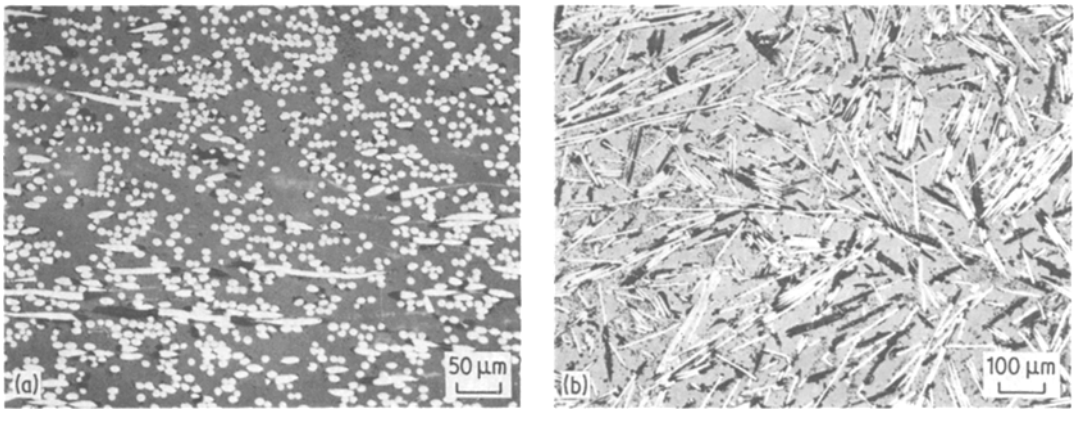

Figure 3 Normal to ply plane (a) and in-plane composite microstructure for Celion graphite-reinforced borosilicate glass. glass.

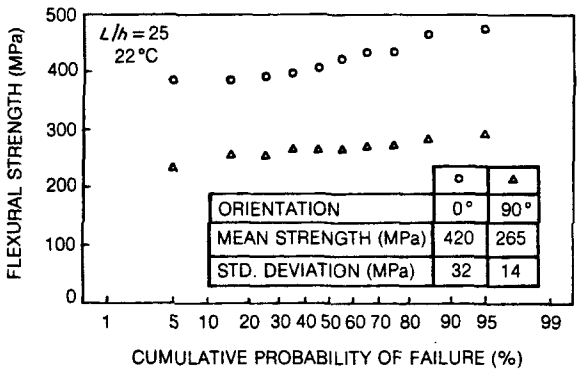

Figure 4 Three-point flexural strength populations for 0° and 90° oriented Celion graphite-reinforced borosilicate glass.

balance borosilicate glass. The average per ply thickness in the bonded composites was approximately 50 μm.

3.2. Three-point bend testing

The three-point bend flexural-strength values obtained from two composite panels are presented in Fig. 4. Each panel was cut into 10 specimens with the distinction between these two specimen groups being their orientation. It was found that, although the fibre orientation distribution appeared random in the paper plane, there was a significant tendency for alignment parallel to the length of the graphite paper roll. This was, for convenience, referred to as the 0° direction while the direction parallel to the roll axis is referred to as the 90° direction. The data in Fig. 4 clearly demonstrate a significant difference in strength between these two directions. In both cases, however, the strength distributions are quite narrow. Composite elastic modulus also varied with orientation. The average 0° elastic modulus (obtained from the curves of load against specimen deflection in three-point bend) was measured to be 57 GPa while the 90° elastic modulus was 48 GPa. The data in Fig. 5 include those of Fig. 4 as well as additional data obtained from specimens taken parallel to 0°, 45° and 90° from a single composite panel. It is shown that the strength decrease is gradual over the entire angular range.

Flexural strength (measured for specimen $L/h = 30$) was found to be relatively insensitive to test temperature, Fig. 6. In this case 0°-oriented specimens were tested in air over the range 22 to 450° C without noticeable alteration in composite performance or failure mode.

Composite three-point bend shear strength ($L/h = 5.5$) was also measured as a function of

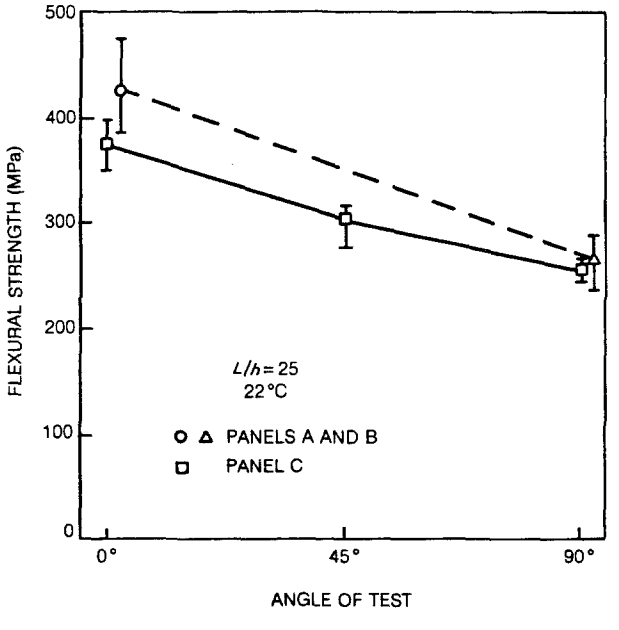

Figure 5 Three-point flexural strength as a function of in-plane orientation for Celion graphite-reinforced borosilicate glass.

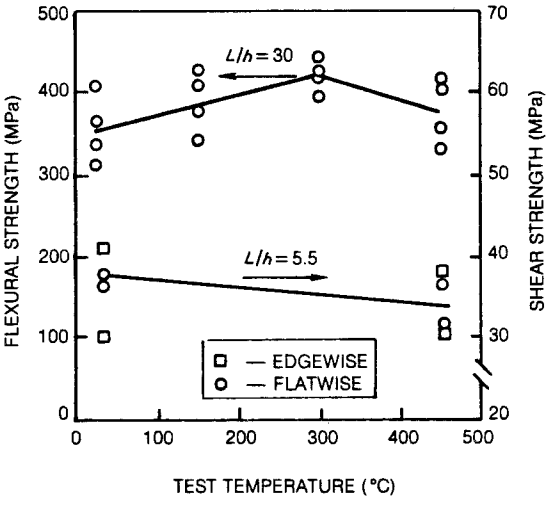

Figure 6 Three-point bend flexural and shear strength of Celion graphite-reinforced borosilicate glass as a function of test temperature in air.

temperature and in both the flat and edgewise orientations, Fig. 6. It had been expected that interlaminar shear would occur more readily in flatwise oriented specimens as compared to edgewise specimens. The fact that this was not found to be the case may relate to the observation that the specimens did not ultimately fail in pure shear. Very rounded load against deflection curves indicated that some shear-induced failure was probably taking place; however, ultimate composite failure was associated with fracture on the tensile specimen surface.

3.3. Four-point bend testing

The use of the four-point bend test permitted the placement of strain gauges on the tension side of the specimens. Fig. 7 presents the stress (calculated as the maximum flexural stress on the outer surface of the specimen) against strain curve obtained from a strain gauge placed at the centre of the tensile surface of the beam. This curve consists of three very distinct regions. First, there is a linear elastic portion which is characterized by an elastic modulus of 57.4 GPa, which is less than that of even the parent borosilicate glass matrix. At a strain of approximately 0.1% the curve goes through a rapid non-linear decrease in slope to a minimum effective value of 27.6 GPa after which a gradual increase in stress–strain slope takes place which finally culminates in composite fracture at about 1% strain. As will be described later, this behaviour can be described on the basis of matrix microcracking and fibre–matrix debonding.

The data obtained from the testing of 12 four-point bend specimens are presented in Table II. Specimens with as-fabricated (glass-rich) surfaces and specimens with machined (diamond abrasive ground) surfaces were found to provide very similar data. The overall average four-point flexural strength of these specimens is 319 MPa, as compared to an average three-point flexural strength of 357 MPa for specimens taken from the same composite panel. Also listed in the table are data for four specimens which had each been subjected to 50 fatigue cycles prior to ultimate fracture. A typical maximum tensile stress against strain history obtained during the testing of one of these specimens is shown in Fig. 8. The specimen was loaded to a surface stress well beyond the proportional limit stress and then unloaded and reloaded to display the level of elastic modulus retained. The new modulus was found to be 73% of the initial specimen modulus even after the specimen had been loaded to a strain of 0.75% prior to unloading. Fatigue was carried on for 50 cycles between 205 MPa and 25 MPa followed by final bend testing to measure composite residual strength. The average value of residual strength is 307 MPa, which corresponds to 96% of the average for all unfatigued specimens, Table II. This ability

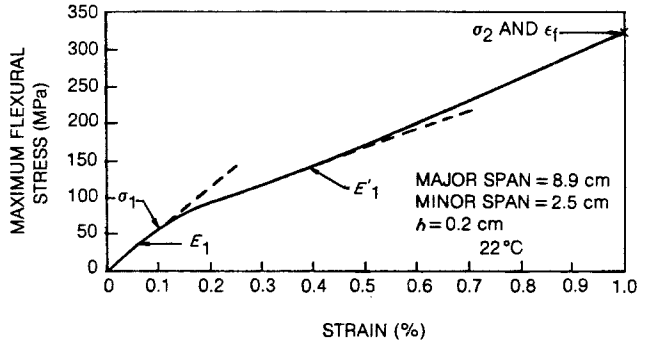

Figure 7 Four-point bend stress–strain behaviour (measured with strain gauge on tension side) for Celion-reinforced borosilicate. $\sigma_1 = 63.4$ MPa, $\sigma_2 = 326$ MPa, $E_1 = 57.4$ GPa, $E_1' = 27.6$ GPa, $\epsilon_f = 1\%$.

TABLE II Celion-reinforced borosilicate four-point bend data at 22°C* (major span = 8.9 cm, minor span = 2.5 cm)

Surface condition	h (cm)	Strength (MPa)	Elastic modulus† (GPa)	Failure strain† (%)
Ground	0.2	337	54.7	–
		306	54.2	0.98
		292	49.6	1.05
		331	54.4	1.11
As-fabricated	0.25	333	58.7	–
		321	51.3	–
		309	59.3	0.94
		326	57.4	0.98
Ground‡	0.2	309	–	–
		276	–	–
		318	–	–
		327	–	1.05

*This composite exhibited an average three-point flexural strength of 357 MPa.
†Measured by strain gauge on tension side.
‡After 50 tension–tension fatigure cycles between 205 and 25 MPa.

to retain original composite strength and a large fraction of the composite elastic modulus is important evidence that, even at this large value of strain and after fatigue, the composite is still a structurally sound material. The necessary presence of matrix microcracks has not diminished overall composite integrity.

3.4. Tension testing

The axial tension testing of strain-gauged specimens resulted in the data presented in Table III and the general stress–strain curve characteristics of Fig. 9. The tensile strength is significantly less than either four-point or three-point bend data; however, the same general features of the stress–strain curve are retained. An initial elastic loading portion is followed by a region of pseudo "work-hardening" followed by fracture. It should be noted that although the ultimate tensile strength is only 47% of the average four-point bend flexural strength, the tensile stress at which initial deviation from elastic linearity occurs (in the tension test) is 70% of that measured in four-point bend. This point relates to the fact that the probable major cause of higher four-point flexural strength is the non-linear deformation of the beam during bending. The maximum flexural stress is calculated on the basis of a linear elastic theory which does not truly apply to the beam once the tensile surface has experienced matrix cracking.

A small number (10) of tension–tension fatigue cycles was applied to two tensile specimens and the residual tensile strength measured. A slight decrease in tensile performance was measured, Table III.

The fracture of the tensile specimens occurred in a fairly localized manner in the regions near or under the glass fibre–epoxy doublers. Evidence of large cracks or incipient failure in other regions of the specimens was not found. Figs. 10 and 11 illustrate the nature of the composite tensile fracture surface and show fibres oriented parallel and perpendicular to the tensile axis which have separated from the surrounding matrix. Fibres in all orientations have cleanly pulled free of the matrix which has cracked around them. At even high magnification (Fig. 12) it is possible to note the very intimate contact that was created between fibres

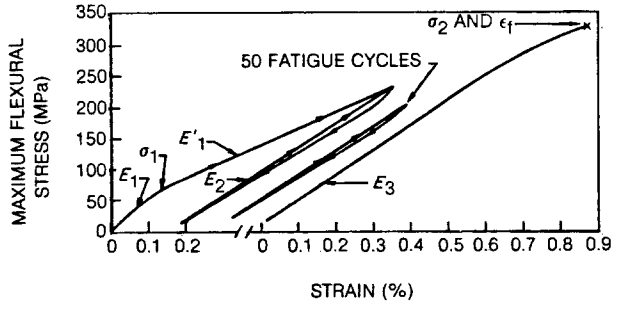

Figure 8 Stress–strain behaviour prior to and after 50 cycles of four-point bend testing (measured with strain gauge on tension side) for Celion-reinforced borosilicate. σ_1 = 54.5 MPa, σ_2 = 327.0 MPa, E_1 = 55.1 GPa, E'_1 = 27.6 GPa, E_2 = 40.5 GPa, E_3 = 40.5 GPa, Total ϵ_f = 1.05%.

TABLE III Celion-reinforced borosilicate* 22°C tensile test data

Condition	Tensile strength (MPa)	Elastic modulus (GPa)	Failure strain (%)
As-fabricated	157	55	0.65
	142	48	0.61
After fatigue†	138	53	0.59
	130	55	0.58

*The average three-point bend flexural strength obtained from five specimens from the same panel is 433 MPa
†10 cycles of tension–tension fatigue between 14 MPa and 100 MPa

and matrix during densification and also the absence of any apparent reaction products at the fibre–matrix interface as a result of the elevated temperature fabrication step.

3.5. Fracture toughness

Prenotched three-point bend specimens (refer to Fig. 2 for geometry of specimens) were tested at 22 and 450°C, Table IV. The specimens were oriented in the edgewise condition so that crack propagation occurred in a direction parallel to the planes of the graphite paper. Composite fracture, by crack propagation, occurred at the same value of applied load, for both temperatures. Fracture-toughness values, calculated using these maximum loads resulted in stress-intensity values of approximately 9 to 11 MPa $m^{1/2}$. Specimens tested in the flatwise orientation, failed in a different manner with extensive interlaminar cracking occurring at the base of the machined notch. It is interesting to note that this mode was more prominent in these notched specimens than in previously tested unnotched specimens with an (L/h) ratio of 5.5. This is probably due to the introduction of high levels of tensile stress normal to the ply plane, as well as shear, at the notch root which enhance the tendency for interply separation.

3.6. Thermal cycling and thermal exposure

Three-point bend configured specimens were subjected to thermal cycling and static thermal exposure in air. In both cases the specimens had been surface-ground prior to test to remove any protective glass surface layer. Thermal cycling took place between 22 and 430°C with heat up, hold and cool down phases of an entire 12 min cycle requiring 4 min each. Although the ambient air for the low-temperature portion of the cycle was at 22°C, the minimum interior specimen temperature achieved was 50°C. The residual three-point flexural strength and specimen mass loss are presented in Fig. 13. While the specimen strength degradation continued over the entire number of cycles, the mass loss appeared to stabilize at a value of about 1.2% after 200 cycles. This overall specimen loss of mass can be translated into a 7% loss of fibre (assuming all mass loss is in oxidation of graphite), however, since it is probably occurring from the specimen surfaces inward it can account for a significantly greater reduction in flexural strength.

Similarly, the static exposure of specimens to air for 100 h at 430°C caused a 7% overall composite mass loss and an 80% loss of composite strength, Table V. In this case the loss of graphite mass would be expected to be 41%.

In contrast to the above oxidation, the immersion of specimens for 24 h in boiling water caused no measurable loss of composite strength, Table V.

3.7. Thermal expansion and thermal conductivity

Composite thermal expansion was measured in the 0° direction in the plane of the composite and also through the thickness, i.e. normal to the paper ply planes. In both cases composite thermal expansion was linear over a temperature range of 22 to 300°C with values of coefficient of thermal exapn-

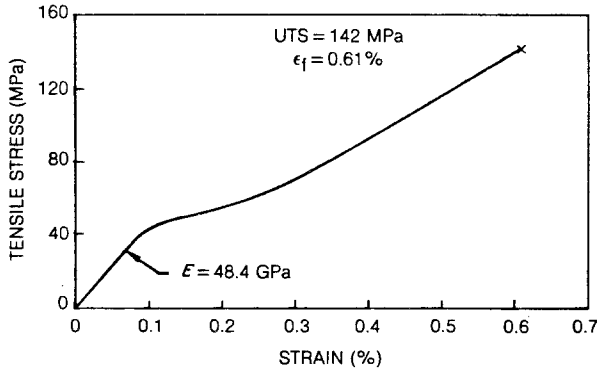

Figure 9 Tensile stress–strain curve at 22°C (measured with strain gauges on tension specimen) for Celion-reinforced borosilicate.

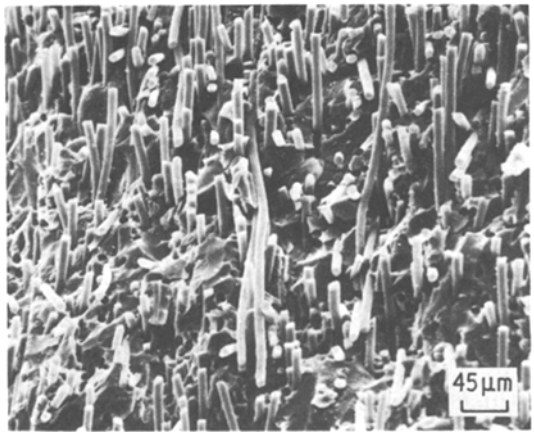

Figure 10 Tensile fracture surface of Celion graphite-reinforced borosilicate glass.

sion (CTE) equal to $1.7 \times 10^{-6}\,^{\circ}C^{-1}$ in the plane and 3.9 to $4.5 \times 10^{-6}\,^{\circ}C^{-1}$ normal to the plane. The thermal conductivity was measured only in the direction normal to the ply plane and its value, at a measurement temperature of 25° C, is 1.04 W $m^{-1}\,^{\circ}C^{-1}$ (0.60 Btu ft $hr^{-1}\,ft^{-2}\,^{\circ}F^{-1}$). The in-plane thermal conductivity, although not measured, would be expected to be larger than this value because of the longer path length of graphite in all in-plane directions and the higher fibre axial thermal conductivity.

3.8. Effect of fibre content on strength and stiffness

While all of the previously described data were obtained for composites having a fibre content of approximately 30 to 35% by volume, several additional composite panels were fabricated with smaller percentages of reinforcement. The three-point flexural strength (Table VI) was found to decrease with decreasing fibre content, however, composite flexural elastic modulus was not altered consistently.

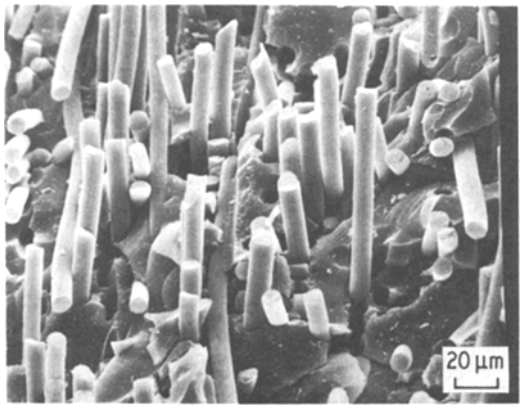

Figure 11 Tensile fracture surface of Celion graphite-reinforced borosilicate glass.

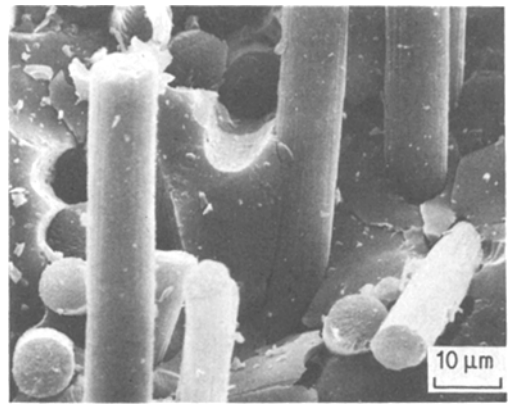

Figure 12 High magnification view of fibre–matrix interface for Celion graphite-reinforced borosilicate glass.

3.9. Effect of fibre length on strength and stiffness

While an extensive investigation of the importance of individual fibre length was not undertaken, several composite panels were fabricated with fibres of shorter length than the 1.9 cm standard (Table VII). At the time that this work was performed, Celion graphite fibre papers containing fibres of 1.25 and 0.63 cm length were the only other available candidates. In one case (Table VII), a 50%/50% mix of these two fibre lengths in a paper-reinforced composite produced the same elastic modulus as the 1.9 cm long fibres; however, there was nearly a 15% drop in flexural strength. A much greater strength drop was registered when the fibre length was decreased to all fibres having a length of 0.63 cm. Even with a higher fibre content, the composite strength was substantially reduced and was accompanied by a 20% reduction in stiffness.

4. Experimental results—effect of matrix and fibre composition

4.1. Fibre

A higher elastic modulus graphite fibre, Fortafil 5, was used to reinforce borosilicate glass and found to have substantial effects on strength, stiffness and thermal expansion behaviour (Table VIII). The composite stiffness was increased by 35% over that of Celion fibre-reinforced composite. While the axial coefficient of thermal expansion (CTE)

TABLE IV Three-point bend of prenotched specimens* of Celion-reinforced borosilicate

Test temperature (°C)	Orientation	h (cm)	c (cm)	K_c (MPa m$^{1/2}$)	Failure mode
22	Edgewise	1.0	0.2	11.0	Crack
22		1.0	0.2	11.2	Crack
450		1.0	0.2	10.4	Crack
22	Edgewise	0.5	0.2	8.7	Crack
22		0.5	0.2	8.8	Crack
22	Flatwise	0.5	0.2	7.7	Shear
22		0.5	0.2	8.5	Shear

*Test span (L) of 5 cm.

of the Celion fibre is already negative, the higher elastic modulus of the Fortafil fibre is also probably accompanied by an even more negative fibre axial CTE. These two properties have combined to reduce the composite CTE by nearly 50% (Table VIII).

Finally, composite strength was greatly reduced despite the fact that the fibre manufacturers' data indicate only a slight difference in fibre strength. These findings were not examined further but, particularly in the case of composite strength, point to a major difference in translation of fibre properties to composite performance.

4.2. Matrix

The principal effect of altering composite matrix composition was to change the dependence of composite strength on test temperature. While other lesser changes also took place (Table VIII), very significant increases in high-temperature performance were achieved (Fig. 14) by using glasses with significantly higher thermal stability (Table I). The three-point flexural strength data were obtained by testing at temperature in an argon atmosphere to avoid the fibre oxidation problems described in Section 3.6. The borosilicate, aluminosilicate and 96% silica matrix composites were all fabricated with 1.9 cm long Celion fibre reinforcement and all were tested at temperatures high enough to finally reach a level above which excess composite softening occurred.

For the borosilicate matrix composite specimens, containing 22 vol% reinforcement, a sharp decrease in strength occurred above 500° C (Fig. 14). This was accompanied by a gradual change in failure mode from fracture, below 500° C, to simply composite bending at 700° C. At this highest temperature the matrix viscosity has decreased to a level of approximately 10^{10} P which is sufficiently low to permit extensive matrix deformation.

For the aluminosilicate glass matrix composites, containing 32 vol% reinforcement, the same transition in failure mode occurred. However, in this case the drop in flexural strength did not occur until the test temperature exceeded 700° C. This was expected since this glass softens at a higher temperature than the borosilicate (Table I). Another significant feature of performance for this composite is the very marked increase in composite flexural strength with increasing temperature between 22° C and 600° C. This 30% increase in strength with increasing temperature is probably related to an increase in tensile failure

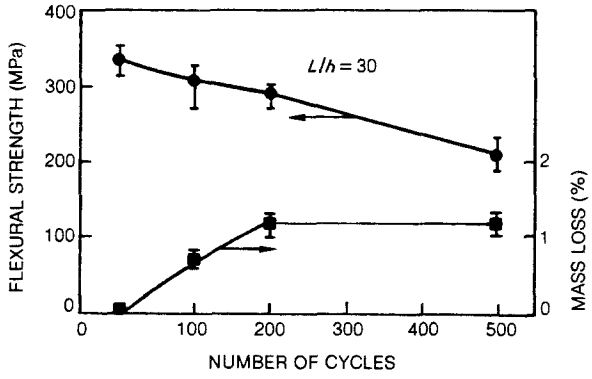

Figure 13 Three-point flexural strength at 22° C after thermal cycling in air between 22 and 430° C for Celion graphite-reinforced borosilicate glass.

TABLE V Effect of environmental exposure conditons on flexural strength Celion-reinforced borosilicate

Exposure condition	Three-point flexural strength (MPa) (Average of 6 tests)
As-fabricated	358
100 h in air at 430° C	73
As-fabricated	307
24 h in boiling water	340

strain, or decrease in tensile proportional limit stress of the composite which would permit a larger load to be carried in bending prior to failure. Also, because the true tensile stress–strain curve is non-linear, the observed flexural strength is probable somewhat in error and the separate effects of failure strain and strength cannot be separated by a simple three-point bend test. The probable change in stress–strain behaviour with temperature is confirmed by the observed change in composite flexural elastic modulus (Fig. 15). Over the 22 to 600° C temperature range in which composite strength increased, the flexural stiffness decreased by 33% indicating that a larger fraction of the three-point bend beam is deforming in the region beyond the composite proportional limit.

The 96% SiO_2 glass-matrix composites, reinforced with 21% by volume fibre, retained their strength to approximately 1000° C. Above this temperature excessive deformation caused a decrease in load-carrying capability.

5. Discussion of results and comparison with an epoxy-matrix composite and unreinforced epoxy

5.1. Comparison with an epoxy-matrix composite

During the period of time that these glass-matrix composites were fabricated, a series of epoxy resin-matrix composites were also created and tested at our laboratory. The properties of these composites are described in greater detail elsewhere [12]; however, a brief summary of the data (Table IX) can provide a useful comparison with glass-matrix composite performance. Unfortunately, a complete set of data are not available for composites containing approximately the same fibre content.

As would be expected, glass-matrix composite density is considerably higher than that of the epoxy-matrix counterpart; measured values agree well with a straightforward rule of mixtures calculation.

A better appreciation for the difference in composite stress–strain behaviour can be obtained through the comparison of composite tensile curves (Fig. 16).

The glass-matrix composite tensile elastic modulus is found to be considerably larger than the value for the epoxy-matrix composite due primarily to the higher stiffness of the glass matrix. The following approximation can be used for the elastic modulus of a two-dimensional mat of discontinuous fibres [13, 14] where E and V refer to elastic modulus and volume fraction and and the subscripts c, f and m refer to composite, fibre and matrix, respectively:

$$E_c = 3/8E_fV_f + E_mV_m. \quad (1)$$

For the Celion graphite fibre-reinforced epoxy matrix composite a calculated value of 20.8 GPa is in reasonably good agreement with the measured value of 18.2 MPa (Table IX). There is a complete lack of agreement, however, in the case of the glass-matrix composite where a calculated value of 70.4 GPa far exceeds the measured value of 52 MPa. It is particularly interesting to note that the value of E_c, in this case, is less than that of E_m. As a lower bound, Cox [14], derived an expression for the stiffness of a two-dimensional random mat of fibres that was unconstrained by any matrix:

$$E_c = 1/3E_fV_f. \quad (2)$$

Use of this equation shows that the presence of the matrix provides a substantial increase in stiffness above the lower bound value of 23.4 GPa. A

TABLE VI The effect of fibre content on the performance of Celion-reinforced borosilicate

Vol%			Flexural strength* (MPa) Av./STD dev.	Flexural modulus* (GPa) Av./STD dev.
Fibre	Glass	Porosity		
21	78	1	310/15	49/2.2
17	82	1	282/11	50/4.0
15	84	1	234/23	55/1.1
12	88	0	224/9	48/1.5

*Five specimens of each type tested at $L/h = 30$.

TABLE VII The effect of fibre length on the performance of Celion-reinforced borosilicate

Fibre length	Vol %			Average flexural data*	
	Fibre	Glass	Porosity	Strength (MPa)	Modulus (GPa)
1.9	22	77	1	335	48
50%–1.25 cm 50%–0.63 cm	22	74	4	289	48
0.63 cm	27	67	6	186	40.6

*Three-point bend testing at $L/h = 25$. In each case an average of 6 specimens tested.

possible explanation for this inability to achieve predictive agreement for the glass-matrix composite may lie in an assumption that the graphite fibres and/or glass-matrix have not been degraded during glass-matrix composite fabrication. Matrix degradation could take place in the form of matrix microcracking during cooling of the composite from the fabrication condition. The Celion graphite fibres have a negative axial CTE value of approximately $-0.5 \times 10^{-6}\,^{\circ}C^{-1}$ near room temperature. While the author is unaware of fibre CTE data at elevated temperatures, the CTE value is certainly significantly less than that of the borosilicate glass over the 22 to 560° C (borosilicate glass annealing point – Table I) temperature interval that represents the thermal cooling range (after composite densification) over which significant residual stresses can be generated. For the borosilicate, aluminosilicate and 96% SiO_2 glasses, matrix contraction strain during cooling from their particular annealing points to 22° C is calculated to be 0.18%, 0.33% and 0.07%, respectively. Opposed by at least some axial expansion of the fibres during this cooling, and in the presence of the many fibres situated as stress raisers, it is reasonable to expect that matrix microcracking could take place and cause an effective decrease in matrix stiffness. Using Equation 1 it would require that the effective borosilicate matrix stiffness would have been reduced from 63 MPa to approximately 37 MPa.

Metallographic examination of the composite microstructure, however, did not reveal the presence of a large population of microcracks. Instead the matrix appeared relatively crack-free requiring the need for another plausible explanation. This may be found in the very low transverse properties of unidirectional graphite fibre-reinforced glass-matrix composites [8]. It would appear that no real bond is formed between fibre and matrix and, in fact, it is probable that a gap exists between the fibre and matrix due to the fact that the radial CTE of the graphite fibre is much larger than that of the matrix. A typical graphite fibre radial CTE can be of the order of $20 \times 10^{-6}\,^{\circ}C^{-1}$ illustrating the tremendous anisotropy of graphite fibre CTE and also indicating that, for glass matrices such as those listed in Table I, the fibre can shrink away from the matrix during cooling. By use of this fact and an approximate equation attributed by Bert [15], to Halpin and Tsai, another estimate of discontinuous fibre reinforcement can be made:

$$E_c = 3/8E_L + 5/8E_T. \quad (3)$$

In this case E_L and E_T are the axial and transverse elastic moduli of a unidirectional continuous fibre-reinforced composite containing the same percentages of constituents as the discontinous fibre-reinforced composite. It follows that Equation 3 can be rewritten:

$$E_c = 3/8(E_f V_f + E_m V_m) + 5/8E_T. \quad (4)$$

Using Equation 4 it is anticipated that for the glass-matrix composite an appropriate value of E_T would be 16 MPa. This value is probably reasonable since, from the above discussion of radial expansion mismatch, the unidirectional composite

TABLE VIII Effect of matrix and fibre composition on composite properties at 22° C

Glass matrix	Borosilicate	Borosilicate	Aluminosilicate	96% silica
Fibre type	Celion 6000	Fortafil 5	Celion 6000	Celion 6000
Fibre content (vol %)	22	22	32	21
Three-point flexural strength (MPa)	335	222	330	286
Flexural elastic modulus (GPa)	48	65	45	45
Coefficient of thermal expansion at 22° C ($10^{-6}\,^{\circ}C^{-1}$)	1.7	0.9	–	0.5

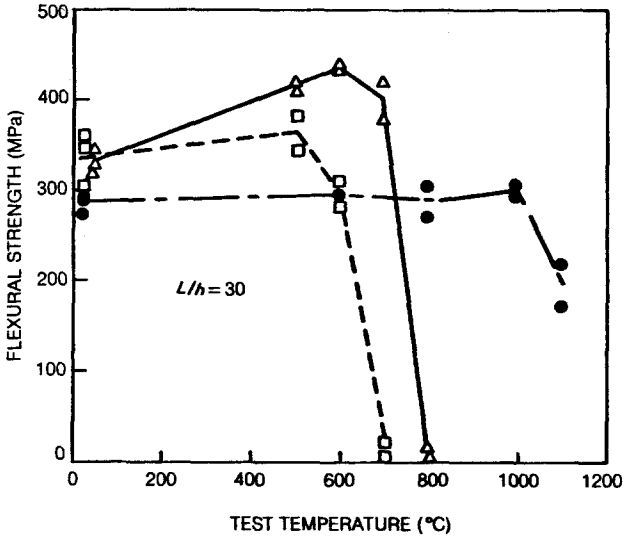

Figure 14 Three-point flexural strength for Celion graphite fibre-reinforced glass specimens tested at temperature in argon: □ – borosilicate glass matrix with 22 vol% fibre; △ – aluminosilicate glass matrix with 32 vol % fibre; • – 96% SiO_2 glass matrix with 21 vol% fibre.

analogue could be considered to consist of a glass-matrix containing 30% porosity, [16, 17].

This transverse property description may also help to explain the lack of dependence of E_c on V_f observed in Table VI. While a decrease in fibre content would be expected to cause a decrease in E_c, even if the fibres had been degraded during fabrication, this was not found to be the case. The relative invariance of E_c may relate to an accompanying increase in E_T with a decrease in fibre content causing the increased transverse performance (E_T) to offset any loss of fibre contribution to E_L.

The most distinctive difference in stress–strain behaviour between the two composite systems (Fig. 16), is the fact that the glass-matrix composite goes through, at least in part, a facsimilie of the three-region behaviour described previously in Fig. 1 while the epoxy-matrix composite exhibits a completely linear stress-strain curve up to failure. The major difference between these two composites that can cause this distinction can be found in the failure strains of the two matrices. In the case of the epoxy-matrix system, the matrix failure strain exceeds that of the fibres and hence composite failure occurs through the sequence of fibre fracture followed by matrix failure. In the case of the glass-matrix composite, at a composite tensile strain of approximately 0.075% it is postulated that matrix failure becomes extensive through the mechanism of microcracking as described by Aveston [18, 19] and others [10, 11]. Progressive matrix cracking causes the region 2 (Fig. 1) type of reduced stress–strain slope which should terminate once the matrix has broken into microcracks whose spacing is dictated by the ability of the fibres to carry the load across the microcrack gaps and the length of matrix required to transfer load to the fibres. The increment of composite tensile strain, $\Delta\epsilon_c$, that should be attributable to this process can be given by the following expression [18, 19]:

$$\Delta\epsilon_c = \frac{\alpha\epsilon_{mu}}{2} \tag{4}$$

where

$$\alpha \approx \frac{E_m V_m}{\eta E_f V_f}, \tag{5}$$

and ϵ_{mu} = matrix failure strain. The factor η is taken as approximately 0.25 for a two-dimen-

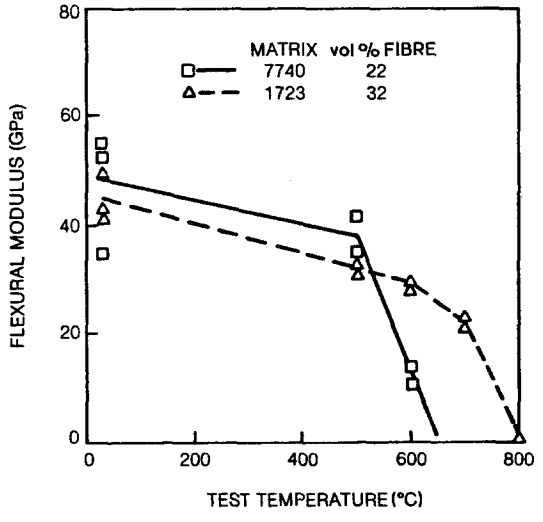

Figure 15 Three-point flexural elastic modulus of Celion graphite fiber-reinforced glass-matrix composites as a function of test temperature.

TABLE IX Comparison of Celion fibre-reinforced glass- and epoxy-matrix composite properties at 22° C

Matrix	Epoxy	Borosilicate	Glass
Fibre content (vol%)	20	30–35	21
Density (g cm^{-3})	1.31–1.36	2.0	–
Average tension strength (MPa)	180	150	–
elastic modulus (GPa)	18.2	52	–
failure strain	0.06	0.63	–
Average three-point flexural strength (MPa)	268	400	310
In-plane Coefficient of thermal expansion between 22 and 150° C (10^{-6} °C^{-1})	21–32	1.7	–
Short-beam shear strength			
Flatwise	>52.4	>37.5	–
Edgewise	>63.4	>35.5	–

sional random array of discontinuous fibres of length greater than the critical transfer length [13]. Using these expressions it is predicted that the failure strain increment, $\Delta\epsilon_c$, for region 2-type behaviour should be approximately $0.23\epsilon_{mu}$. In the case of the tensile stress–strain curve in Fig. 16, where first evidence of cracking occurs at a strain 0.075%, this corresponds to a strain increment of 0.017%. Thus, the high stiffness of the reinforcing fibres precludes the presence of a significant region 2-type of behaviour and, as seen in Fig. 16, a truly horizontal stress–strain segment is not observed.

As shown in Table III, the composite tensile elastic modulus is not decreased significantly after several mechanical fatigue cycles to 67% of its as-fabricated ultimate strength. This would also agree with the contention that additional matrix microcracking has a minimal effect on composite performance. In contrast, the decrease in stiffness noted in Fig. 8 for bend-tested specimens may relate to the much higher strains achievable in bending as discussed next.

Comparison of epoxy- and glass-matrix composite flexural strengths (Table IX) reveals that, in contrast to the tensile data, the glass-matrix material exhibited a much higher load-carrying capability. While the ratio of flexural strength to tensile strength is 1.5 for the epoxy-matrix composite, it is 2.7 for the glass-matrix counterpart. As shown in the table, a borosilicate-matrix composite containing near the same percentage of fibre-reinforcement exhibited a flexural strength much closer to that of the epoxy, however, no tensile-strength data were available for this composite. The high glass-matrix composite flexural strength can be related to the non-linear tensile stress–strain curve for this material. The value of flexural strength, σ, reported in Table IX is obtained by using the following standard linear elastic formula:

$$\sigma = 3/2\frac{PL}{bh^2} \tag{6}$$

where b represents specimen width and the other quantities are described in Fig. 2.

However, since the glass-matrix composite exceeds its tensile proportional limit after an initial stress of approximately 40 MPa, the use of Equation 6 is no longer appropriate for the calculation of higher stresses. It is interesting to note at this point that, while the ratio of ultimate strength in flexure to that in tension is 2.7, a similar ratio based on the proportional limit stress is only approximately 1.5. This gives greater support to the argument that the

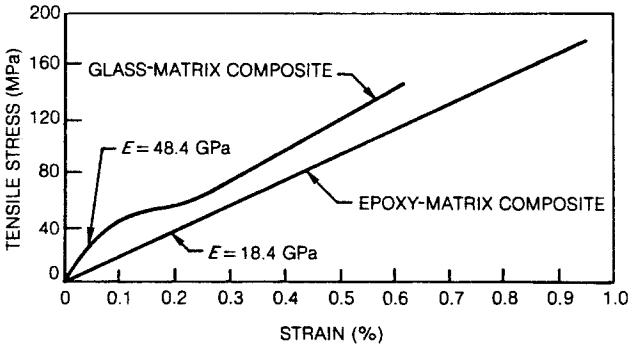

Figure 16 Comparison of tensile test stress–strain curves for discontinuous Celion graphite fibre-reinforced composites. The expoxy matrix composite contains 20% fibre and the borosilicate glass-matrix composite contains approximately 30% fibre.

non-linear stress–strain behaviour beyond the proportional limit is responsible for the large increase in flexural load-carrying capability.

If it is assumed that the compression stress–strain curve for this glass-matrix composite is nearly linear to failure, and that the tensile curve is as shown in Fig. 16, then it can be shown [18, 19], that the composite flexural strength to tensile strength ratio can reach values as high as 3.0. This occurs by virtue of the ability of the composite to "yield" in tension and distribute the applied load more effectively over a larger fraction of the flexural specimen thickness. This causes a change in the position of the specimen neutral axis toward the compression face. Thus, by deforming beyond the proportional limit the glass-matrix composite is much more effective at carrying a load in bending than its linear elastic epoxy-matrix composite counterpart.

5.2. Comparison with unreinforced glasses

A summary of composite properties, along with those of a borosilicate glass and several glass-ceramics, is provided in Table X. It is apparent that the graphite-reinforced glass has as its major advantages its high-strength, failure strain and fracture toughness. In the cases of the other materials, values of tensile strength, failure strain, and fracture toughness are generally unavailable in the literature. This is because of the brittle nature of these materials. In most cases their tensile failure strain would be 0.1 to 0.2%.

A comparison with a machinable glass ceramic is of particular interest because the graphite fibre-reinforced glass composite is also machinable. Fig. 17 illustrates the detail possible by turning an initially rectangular composite rod in a lathe and machining with a single-point tool. The composite has sufficient fracture toughness to permit this type of treatment without shattering. Other experiments not described here have also demonstrated that electrical discharge machining (EDM) techniques can also be used by virtue of the composite's limited electrical conductivity. Also, the ability to form shapes has been demonstrated by the creaction of hat sections by either hot-pressing directly to shape or reforming preconsolidated flat plates (Fig. 18).

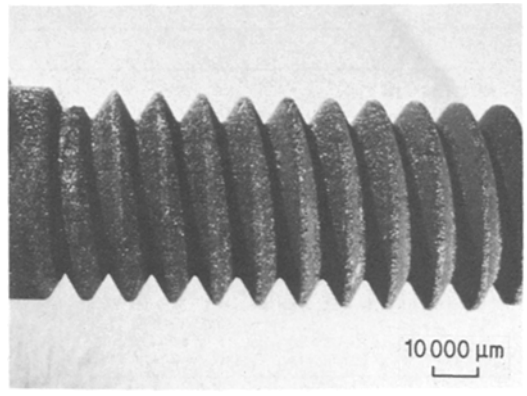

Figure 17 Bolt threads machined by a single-point tool in discontinuous Celion graphite fibre-reinforced borosilicate glass.

6. Conclusions

1. It has been demonstrated that a two-dimensional array of discontinuous graphite fibres can be utilized to effectively reinforce glass matrices. Both composite strength and failure strain far exceed those of the parent matrix.

2. Composite tensile behaviour is characterized by a highly non-linear stress–strain curve. By virtue of this non-linearity, the composite is able to redistribute applied stresses to achieve a high load-carrying capability.

3. The fibrous microstructure and low fibre–

TABLE X Comparison of graphite-fibre-reinforced glass with other glasses

Material	Graphite/ glass composite	Borosilicate glass	Glass-ceramics	
			Machinable	LAS
Density ($g\,cm^{-3}$)	2.0	2.23	2.5	2.6
In-plane tensile strength (MPa)	150	–	–	–
elastic modulus (GPa)	52	62	64	120
failure strain (%)	0.6	–	–	–
Three-point flexural strength (MPa)	325–400	6–60	103	140
Fracture toughness ($MPa\,m^{1/2}$)	10	–	–	–
In-plane CTE ($10^{-6}\,°C^{-1}$) at 25° C	1.7	3.5	12.3	4.0+
Normal to plane CTE ($10^{-6}\,°C^{-1}$) at 25° C	4.2	3.5	12.3	4.0+
Normal to plane thermal conductivity ($W\,m^{-1}\,°C^{-1}$)	1.04	0.97	1.68	3.4
Machinable	Yes	No	Yes	No

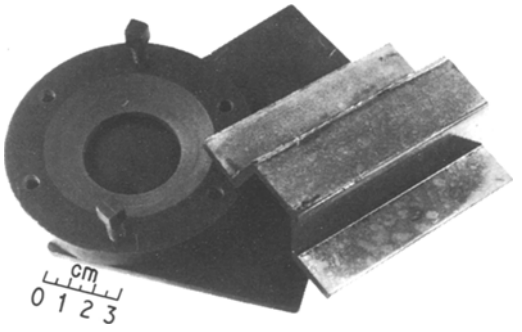

Figure 18 Hot-pressed and machined articles of discontinuous graphite fibre-reinforced glass.

matrix bond strength provide a mechanism for achieving high fracture toughness and also machinability with single-point tools.

4. Composite stability at elevated temperatures in an oxidizing atmosphere is severely limited by the loss of graphite fibres. However, in an inert atmosphere composite-strength retention is limited by the matrix. For a 96% silica matrix composite, strength was retained to over 1000° C.

Acknowledgement

The author is pleased to acknowledge the support of the National Aeronautics and Space Administration Langley Research Center, Hampton, Virginia, USA, for a portion of the work described.

References

1. K. M. PREWO and J. J. BRENNAN, *J. Mater. Sci.* **15** (1980) 463.
2. K. M. PREWO and J. J. BRENNAN, *ibid.* 17 (1982) 1201.
3. J. J. BRENNAN and K. M. PREWO, *ibid.* **17** (1982) 2371.
4. R. A. SAMBELL, A. BRIGGS, D. C. PHILLIPS and D. H. BOWEN, *ibid* 7 (1972) 676.
5. D. C. PHILLIPS, R. A. J. SAMBELL and D. H. BOWEN, *ibid* 7 (1972) 1454.
6. S. R. LEVITT, *ibid* 8 (1973) 793.
7. K. M. PREWO, E. R. THOMPSON, NASA Contract Report 165711, "Research on Graphite Fiber Reinforced Glass Matrix Composites", May 1981.
8. K. M. PREWO, J. F. BACON and D. L. DICUS, *SAMPE Q.* **10** (1979) 42.
9. R. A. SAMBELL, D. H. BOWEN and D. C. PHILLIPS, *J. Mater. Sci.* 7 (1972) 663.
10. A. J. MAJUMDAR, B. SINGH and T. J. EVANS, *Composites,* **12** (1981) 177.
11. D. C. HUGHES and D. J. HANNANT, *J. Mater. Sci.* **17** (1982) 508.
12. K. M. PREWO, Proceedings of the 25th National Exhibition of the Society for the Advancement of Materials and Process Engineering, SAMPE, Azusa, California (1980).
13. V. LAWS, *J. Phys. D. Appl. Phys.* **4** (1971) 1737.
14. H. L. COX, *Brit. J. Appl. Phys.* **3** (1952) 72.
15. C. W. BERT, Presented at the 34th Annual Conference of the Reinforced Plastics/Composites Institute, New Orleans, Louisiana, January (1979).
16. J. K. McKENZIE, *Proc. Roy. Soc. Lond.* **63B** (1950) 2.
17. R. L. COBLE and W. D. KINGERY, *J. Amer. Ceram. Soc.* **39** (1956) 377.
18. J. AVESTON, J. MERCER and J. M. SILLWOOD, National Physical Laboratory, Report No. SI-90-11-98, Januray (1975).
19. D. J. HANNANT, "Fibre Cements and Fibre Concretes" (Wiley, New York, 1978).

Received 21 April
and accepted 25 April 1982